OBSERVATION OF THE DECAY MODE $K_L \to \pi^+\pi^-e^+e^-$

Noboru Sasao
Department of Physics
Kyoto University, Kyoto 606, Japan

Representing the E162/CP Collaboration

ABSTRACT

The decay mode $K_L \to \pi^+\pi^-e^+e^-$ may provide an interesting testing ground for CP violation. A theoretical model predicts a branching ratio of $\sim 3 \times 10^{-7}$ and a CP-violating asymmetry of $\sim 14\%$. Experimentally, only an upper limit has been established so far.

We have conducted an experimental search for the decay mode with the 13-GeV/c proton synchrotron at KEK. We have observed 12 ± 5 events, and obtained the branching ratio of $\mathrm{Br} = (5 \pm 2) \times 10^{-7}$ (preliminary) for this decay mode. In this report, we describe in detail results of the experiment.

1 Physics Motivation

The rare decay $K_L \to \pi^+\pi^-e^+e^-$ may provide an interesting testing ground to investigate CP violation. It is expected to occur via a $\pi^+\pi^-\gamma^*$ intermediate state converting the virtual photon into an e^+e^- pair. Figure 1 shows Feynman diagrams relevant to the decay. There are two dominant amplitudes for the process: an internal Bremsstrahlung (IB) associated with the $K_L \to \pi^+\pi^-$ mode and a direct magnetic dipole (M1) transition. The virtual photons for these two amplitudes have different CP properties; the former is CP even while the latter is CP odd. Thus, their interference gives rise to CP-violating effects. One may establish

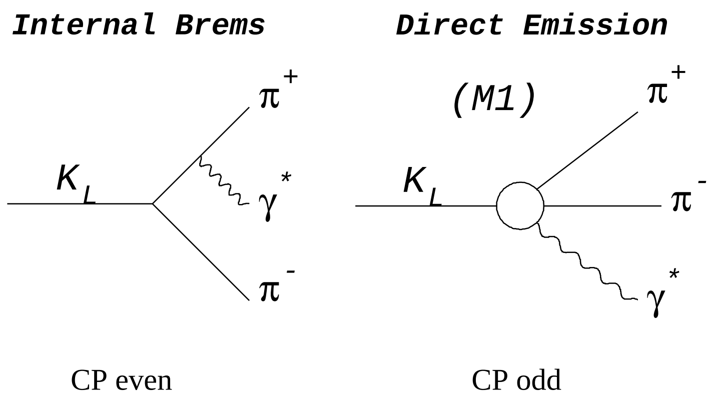

Fig. 1. Feynman diagrams.

it, for example, by observing the $\sin\varphi$ dependence in the decay rate, where φ represents the angle between the planes defined by e^+e^- and $\pi^+\pi^-$ pairs in the K_L rest frame. A theoretical model[1] predicts a branching ratio of $\sim 3 \times 10^{-7}$ and $\sim$ 14% CP-violating asymmetry defined by

$$A = \frac{\int_0^{\pi/2} \left(\frac{d\Gamma}{d\varphi}\right) d\varphi - \int_{\pi/2}^{\pi} \left(\frac{d\Gamma}{d\varphi}\right) d\varphi}{\int_0^{\pi/2} \left(\frac{d\Gamma}{d\varphi}\right) d\varphi + \int_{\pi/2}^{\pi} \left(\frac{d\Gamma}{d\varphi}\right) d\varphi}.$$

(See also Ref. 2.) Experimentally, only an upper limit of Br $< 2.5 \times 10^{-6}$ was reported[3] for the branching ratio. Recently, we have improved the upper limit by a factor of five to Br $< 4.6 \times 10^{-7}$ (Ref. 4) using a part of the data taken in 1996 (Ref. 5). In this article, we report on results of an experimental search for the

$K_L \to \pi^+\pi^-e^+e^-$ decay mode conducted with a proton synchrotron at the High Energy Accelerator Research Organization (KEK).

2 Experimental Setup

The experimental setup is shown schematically in Fig. 2. The main detector was a magnetic spectrometer with a CsI electromagnetic calorimeter at the far end. A brief description will be given below for each component.

2.1 Beam Line

A neutral beam entered the setup from the left in the figure. It was produced by the interactions of 12-GeV/c primary protons with a 60-mm-long copper target at an angle of 2°. The primary beam intensity was about 1×10^{12} protons per spill (lasting nominally two seconds). The divergence of the neutral beam was ± 4 mrad horizontally and ± 20 mrad vertically, defined by a series of collimators embedded in sweeping magnets. A 50-mm-thick lead block was placed at 2.5 m downstream from the target in the beam line to remove γ-rays produced at the target. A 4-m-long decay volume, evacuated down to 10^{-2} Torr, started at 9.5 m downstream from the target.

2.2 Magnet and Drift Chambers

Charged particles were tracked by four sets of drift chambers, two sets upstream (DC1/2) and two sets downstream (DC3/4) of an analyzing magnet. The magnet had an aperture of 900 mm vertically and 2,200 mm horizontally, and provided an average horizontal momentum kick of 136 MeV/c. Each drift chamber set was composed of six readout planes, X-X′, U-U′, and V-V′, in which wires were strung vertically and obliquely by $\pm 30°$, respectively. The cell size was 8 mm $\times$ 8 mm and all the primed planes were staggered by a half-cell to resolve the left-right ambiguity. The chamber gas used was a mixture of Ar(50)-ethane(50). An average position resolution of 200 μm and an efficiency greater than 98% were obtained under a typical running condition. These values became slightly worse in the beam region, where a counting rate exceeded 1 MHz per wire. The overall momentum resolution for 1-GeV/c charged particles was about $\Delta p/p \sim$ 2.5%.

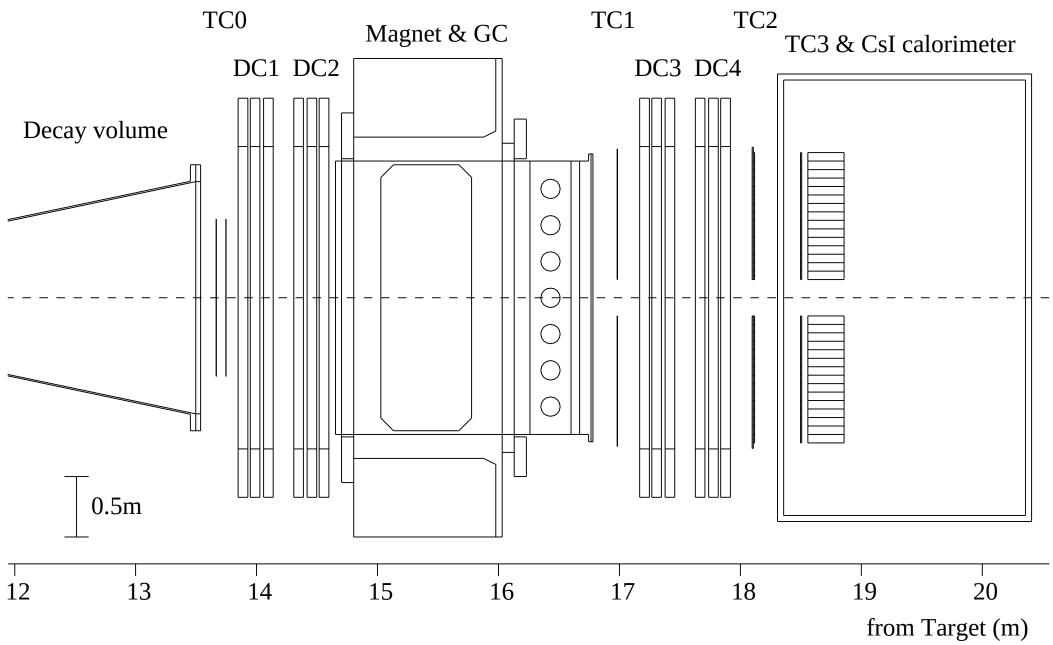

Fig. 2. Schematic plan view of the KEK-E162 detector.

2.3 Gas Cherenkov Counter

A threshold Cherenkov counter (GC), installed inside the magnet gap, was used to identify electrons. The radiator was pure nitrogen at atmospheric pressure, and its effective length was 1.4 m in the beam direction. Cherenkov light was detected by 14 (two vertical by seven horizontal) readout cells; each was equipped with a quasiparabolic reflecting mirror, a light-collecting funnel, and a 5″-quartz-window photomultiplier (Hamamatsu R1251). The mirrors were made from 2-mm-thick acrylic sheets coated with Al and MgF_2 by vacuum evaporation. They were set at an angle of $\pm 45°$ with respect to the horizontal plane and reflected the Cherenkov light onto the photomultipliers located outside the detector aperture. A typical electron efficiency was more than 97% and a pion rejection factor was 400, as determined by K_{e3} event samples.

2.4 CsI Calorimeter

A pure CsI electromagnetic calorimeter, placed at the downstream end of the setup, detected electrons and photons. It consisted of 540 crystal blocks with dimensions of 70 mm $\times$ 70 mm in cross section and 300 mm ($\sim$ 16 X_0) in length. They were arranged into two identical (left- and right-arm) banks, each a matrix of 15 columns and 18 rows. The two banks were placed 300 mm apart horizontally to pass the neutral beam. These blocks were viewed by 2″-photomultipliers (Hamamatsu R4275-02) attached at the downstream end. The temperature of the crystals was kept constant at 25.0 $\pm$ 0.2 °C. The calibration of the energy scale was periodically performed *in situ* using K_{e3} events. Possible changes in the photomultipliers' gain as well as the crystals' transparency were monitored by a Xe-flash-lamp system. The Xe-lamp calibration was performed at a rate of 10 Hz concurrently with the data taking; thus, it enabled interpolation between adjacent calibrations by K_{e3} events. The energy and position resolutions were found to be approximately 3% and 7 mm for 1-GeV electrons, respectively.

2.5 Trigger and Trigger Counter

There were four sets of trigger scintillation counters, called TC0X, TC1X, TC2X/2Y, and TC3X, where X(Y) represented a horizontally (vertically) segmented hodoscope. One set (TC0X) was located immediately downstream of the decay volume, whose active area included the beam region. The other three sets were placed between the magnet and the calorimeter, and had a 300-mm-wide gap at the center for the passage of the beam.

The trigger for the present mode was designed to select events with at least three charged tracks which included at least two electrons. Actually, it was produced at two levels. The decision at level 1 was performed within 100 nsec by NIM logic. The information used was the number of hits in each trigger hodoscope, of GC hits, and of column- and row-hits in the calorimeter, where a column (row)-hit was defined by an analog sum, discriminated at 300 MeV, of energy deposits in each column (row). The decision at level 2 was done within 10 μsec by a set of hardware processors. One processor counted the number of track candidates by looking for the correlated hits in downstream trigger hodoscopes; in addition, it could distinguish electron candidates with GC and column-hit information. Another processor searched for clusters using the hit positions of the CsI blocks. It could distinguish charged and neutral clusters by looking at TC2Y/3X hit positions. The third processor decided whether or not events satisfied the trigger condition for the mode, using the information from the above two processors. Under a typical running condition, the resultant rates for the mode were about 600 and 300 events/spill for the level 1 and level 2 trigger, respectively.

3 Analysis

We have collected approximately 150 million triggers for this decay mode. In order to select the desired events, we screened the raw data in three steps. In the first step, we reconstructed all possible charged tracks and determined their momentum. We then identified the particle species for each track using information from the CsI and Cherenkov counter. We retained event samples consistent with the $\pi^+\pi^-e^+e^-$ topology for further analysis.

In the second step, we looked for the decay mode $K_L \to \pi^+\pi^-\pi^0(\pi^0 \to e^+e^-\gamma)$. For simplicity, we call this mode $\pi^+\pi^-\pi^0_D$ in the following. It has exactly the same decay products as the signal mode apart from the extra γ-ray. In addition, its branching ratio is much bigger. These facts make this decay mode a good normalization process. In the final step, we looked for the signal mode. Here the major task was to reject backgrounds using kinematical constraints. It turned out that the biggest background source was the $\pi^+\pi^-\pi^0_D$ mode, with the final γ-ray escaping detection for one reason or another.

Each analysis step will be explained in more detail below.

3.1 General Event Filtering

The offline analysis started with track finding with drift chamber information. At first, events were required to have at least four tracks with a common vertex in the beam region inside the decay volume. A pion was identified as a track which could project onto a cluster in the calorimeter (a matched track) with E/p < 0.7, where E and p were the energy deposit measured by the calorimeter and the momentum of the track determined by the spectrometer, respectively. An example of the E/p distribution is shown in Fig. 3. An electron was identified as a matched track with E $\geq$ 200 MeV, $0.9 \leq$ E/p ≤ 1.1, and GC hits in the corresponding cells. Having assigned the particle species for each track, we retained the events with four (and

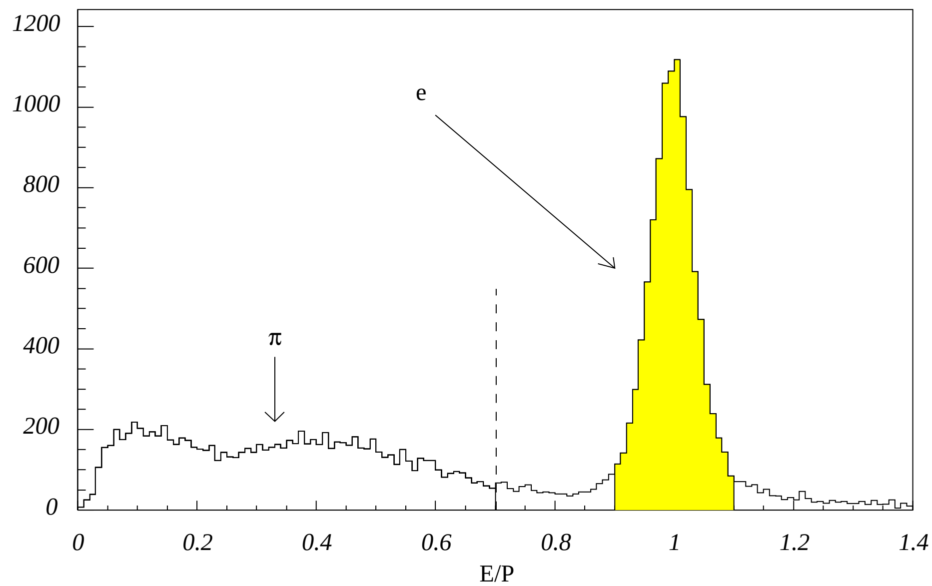

Fig. 3. An example of the E/p distribution.

only four) tracks consistent with the $K_L \to \pi^+\pi^-e^+e^-$ mode. Backgrounds due to nuclear interactions (collisions by neutrons off gas atoms in the decay volume) were reduced by requesting the pion momenta to be less than 4 GeV/c and by limiting the momentum asymmetry $[A_{+-} \equiv (p_{\pi^+} - p_{\pi^-})/(p_{\pi^+} + p_{\pi^-})]$ to be within ± 0.5.

3.2 Normalization Process

Event samples at this stage contained events from the $K_L \to \pi^+\pi^-\pi^0$ ($\pi^0 \to e^+e^-\gamma$) mode. As mentioned, this mode was utilized as a normalization process. Clusters in the calorimeter that did not match with charged tracks were identified as γ-rays. We required the events for this mode to have at least one γ-ray with energy above 200 MeV occurring within ± 3.5 nsec of the event time. If more than one γ-ray existed, we selected the one for which the invariant mass of $e^+e^-\gamma$ ($M_{ee\gamma}$) was closest to the π^0 mass. We further requested the invariant mass of the e^+e^- pair (M_{ee}) to be at least 4 MeV/c^2 to suppress backgrounds from external conversion of γ-rays into e^+e^- pairs. Figures 4(a) and 4(b), respectively, show distributions of the invariant mass of $e^+e^-\gamma$ ($M_{ee\gamma}$) and $\pi^+\pi^-e^+e^-\gamma$ ($M_{\pi\pi ee\gamma}$).

From these plots, we found the mass resolutions for π^0 and K_L to be 5 and 6 MeV/c^2. Figure 5 shows a scatter plot of $M_{\pi\pi ee\gamma}$ vs θ^2, where θ denotes the angle of the reconstructed K_L momentum with respect to the line connecting the production target and decay vertex. The $\pi^+\pi^-\pi^0_D$ events were required to satisfy 3σ cuts; $M_{ee\gamma}$ within ± 15 MeV of the π^0 mass (M_{π^0}), $M_{\pi\pi ee\gamma}$ within ± 18 MeV of the K_L mass (M_{K_L}), and $\theta^2 \leq$ 20 mrad^2, as indicated by the arrows and box in the figures. After all the cuts, 10.3 k events remained. The background contamination was expected to stem mainly from $K_L \to \pi^+\pi^-\pi^0$ ($\pi^0 \to 2\gamma$ with an external conversion), and was estimated to be less than 5% by the Monte Carlo simulation.

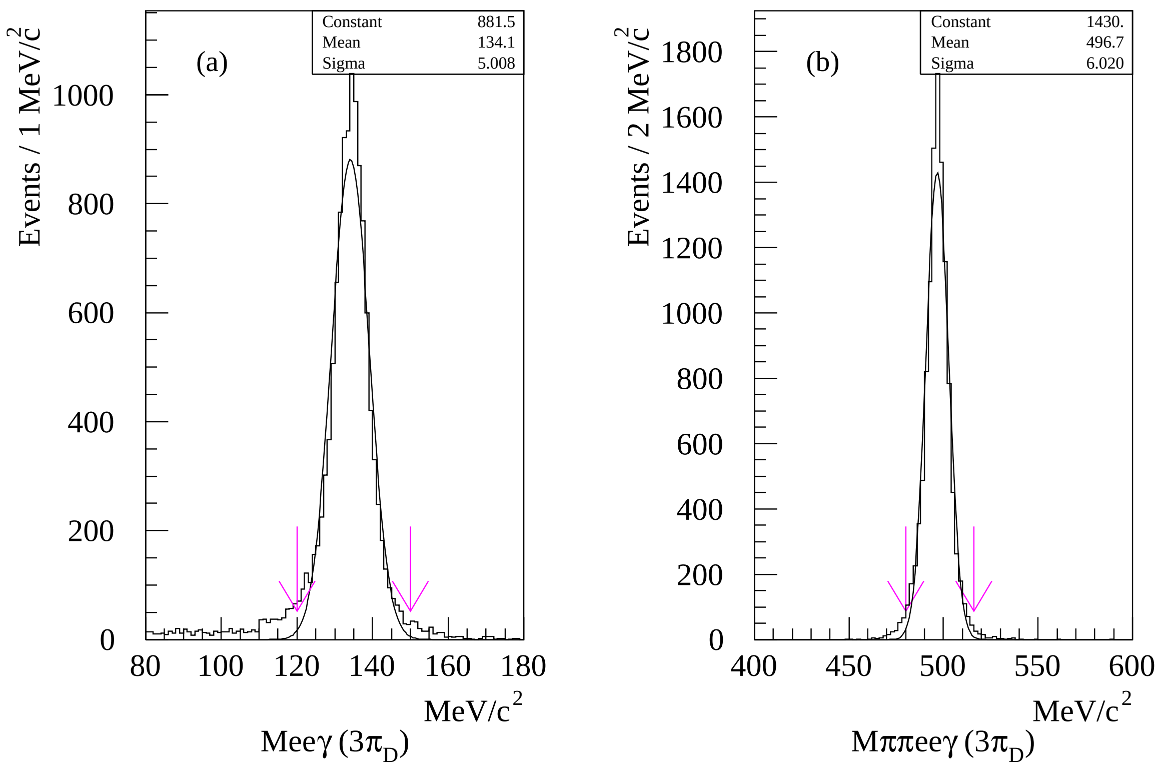

Fig. 4. The invariant mass distribution of (a) $e^+e^-\gamma$ and (b) $\pi^+\pi^-e^+e^-\gamma$ for the $K_L \to \pi^+\pi^-\pi^0_D$ candidates. The events in (a) are required to pass a loose θ^2 cut (≤ 100 mrad^2) as well as all other cuts described in the text. The events in (b) are required to pass the M_{π^0} mass cut in addition to the cuts for the events in (a). The solid lines are Gaussian fits to the data, and the arrows indicate the signal region for the final event samples.

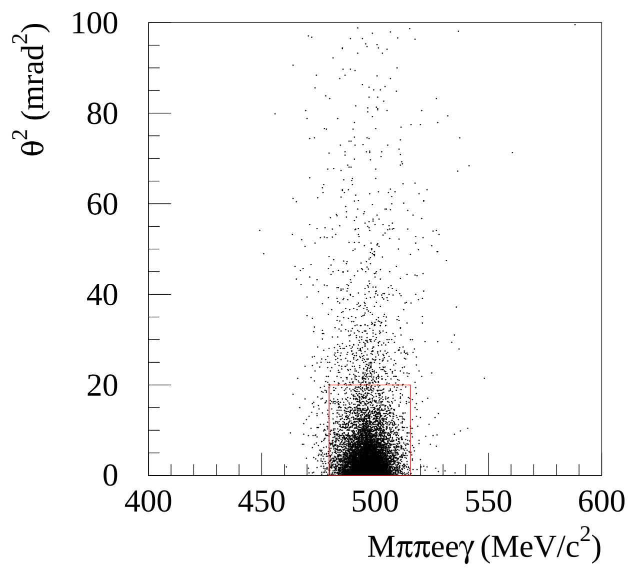

Fig. 5. The scatter plot of θ^2 vs $M_{\pi\pi ee\gamma}$ for the $K_L \to \pi^+\pi^-\pi^0_D$ candidates. The events are required to pass all the cuts, except θ^2 and $M_{\pi\pi ee\gamma}$. The box indicates the signal region.

3.3 Signal Mode

We are now at the stage to identify the $K_L \to \pi^+\pi^- e^+e^-$ mode. In the first place, we removed events which had extra γ-rays consistent with $\pi^0 \to e^+e^-\gamma$. The major background events remaining were those from $\pi^+\pi^-\pi^0_D$ in which the γ-ray was missed. To reject these backgrounds, we chose the following method. First, assuming the existence of a photon with an arbitrary γ-ray momentum $\vec{p}_\gamma$, we defined the parameter χ^2_D:

$$\chi^2_D(\vec{p}_\gamma) = \left(\frac{M_{ee\gamma} - M_{\pi^0}}{\sigma_{M_{\pi^0}}}\right)^2 + \left(\frac{M_{\pi\pi ee\gamma} - M_{K_L}}{\sigma_{M_{K_L}}}\right)^2 + \left(\frac{\theta^2}{\sigma_{\theta^2}}\right)^2 .$$

Here the standard deviations, $\sigma_{M_{\pi^0}}$, $\sigma_{M_{K_L}}$, and σ_{θ^2}, were taken from the experimental distributions for M_{π^0}, M_{K_L}, and θ^2, respectively. The quantity χ^2_D is a measure of consistency for an event with the $\pi^+\pi^-\pi^0_D$ process. We determined

$\vec{p}_\gamma$ by minimizing χ^2_D. If the resultant quantities $M_{ee\gamma}$, $M_{\pi\pi ee\gamma}$, and θ^2 were all within 3σ of their expected values, then we identified the events as $\pi^+\pi^-\pi^0_D$ and rejected them. Figure 6 shows two minimized χ^2_D distributions: (a) Monte Carlo simulation for the $\pi^+\pi^-\pi^0_D$ process, and (b) the actual data sample. The similarity of these plots confirms that the main backgrounds indeed stemmed from the $\pi^+\pi^-\pi^0_D$ process. We finally demanded M_{ee} to be 4 MeV/c^2 or greater, the same condition applied to the normalization mode. Figure 7 shows scatter plots of θ^2 vs the invariant mass of $\pi^+\pi^-e^+e^-(M_{\pi\pi ee})$ after the final cuts: (a) the actual data samples and (b) the Monte Carlo simulation. (Please note that the statistics of the Monte Carlo simulation is about a factor of five larger than the data.) Looking at the plots, we notice that there still remain some background events, especially in the low invariant mass region below $\sim$ 430 MeV/c^2 and the high mass region above $\sim$ 460 MeV/c^2. The mechanism for these events to pass the χ^2_D cut can be understood from the simulation. Those in the low mass region originated from the events in which the electron and/or positron lost its energy by external radiation. If the energy loss occurred before the magnet, the momentum was measured smaller than the actual, resulting in lower invariant mass and large χ^2_D. On the other hand, those in the high mass region originated from the events

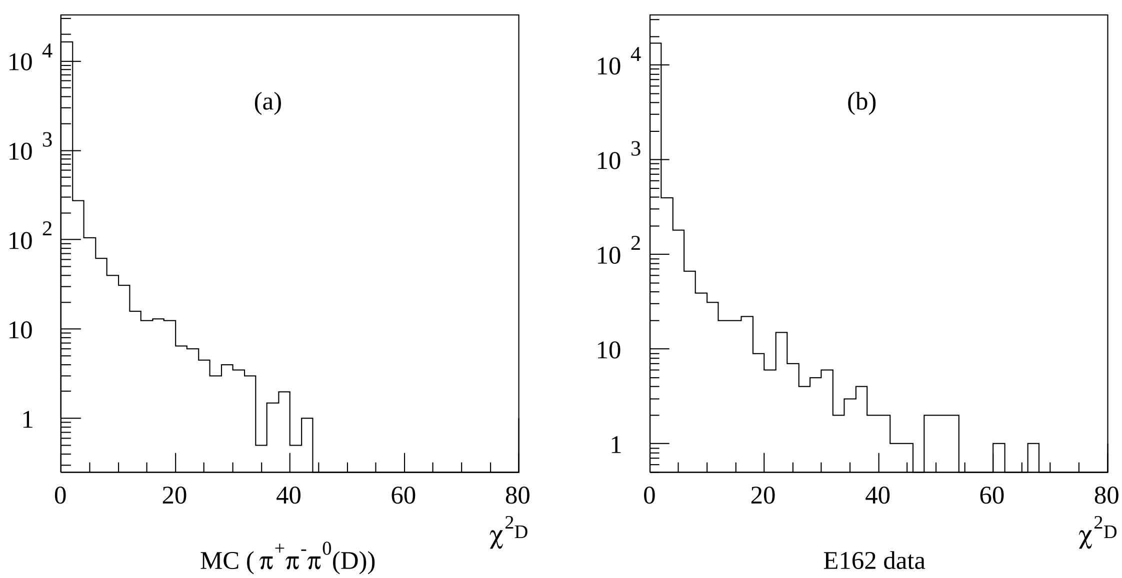

Fig. 6. χ^2_D distributions: (a) Monte Carlo simulation for the $\pi^+\pi^-\pi^0_D$ process and (b) the actual data sample.

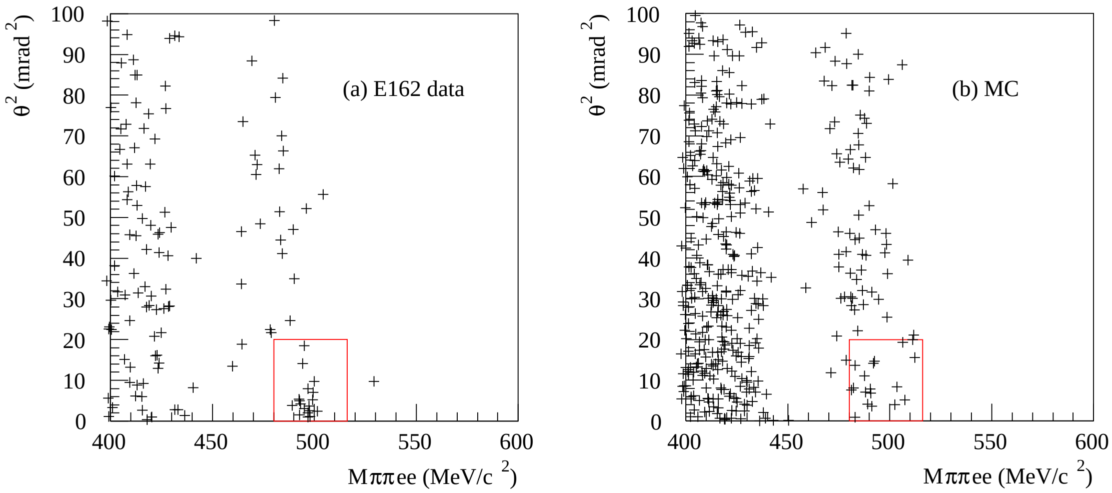

Fig. 7. The scatter plot of θ^2 vs $M_{\pi\pi ee}$ for the $K_L \to \pi^+\pi^-e^+e^-$ candidates: (a) the actual data samples and (b) Monte Carlo simulation for the $\pi^+\pi^-\pi^0_D$ process. The events are required to pass all the cuts, except θ^2 and $M_{\pi\pi ee}$. The box indicates the signal region.

in which one of the pions decayed into muons inside the magnet. In this case, the decayed pion could give a larger momentum than the actual pion, thus resulting in a larger invariant mass.

In order to estimate the background contribution inside the signal box, we adopted the following procedure. Figure 8 shows the projection onto the θ^2 axis of these events with $450 < M_{\pi\pi ee} < 520$ MeV/c^2. We notice that there exists a clear peak at $\theta^2 = 0$ in the actual data (a), but not in the simulation (b). Exploiting a simple and smooth shape observed in the projected curves, we fitted the background shape of the simulation to a straight line. We then renormalized the scale in such a way that the number of actual events in $30 < \theta^2 < 100$ mrad^2 is equal to that underneath the straight line. Then, the events underneath this straight line within $\theta^2 < 20$ mrad^2 were subtracted from the signal. We finally obtained the number of the signal events to be

$$N(K_L \to \pi^+\pi^-e^+e^-) = 12 \pm 5.$$

In the expression above, the error includes only statistical uncertainty.

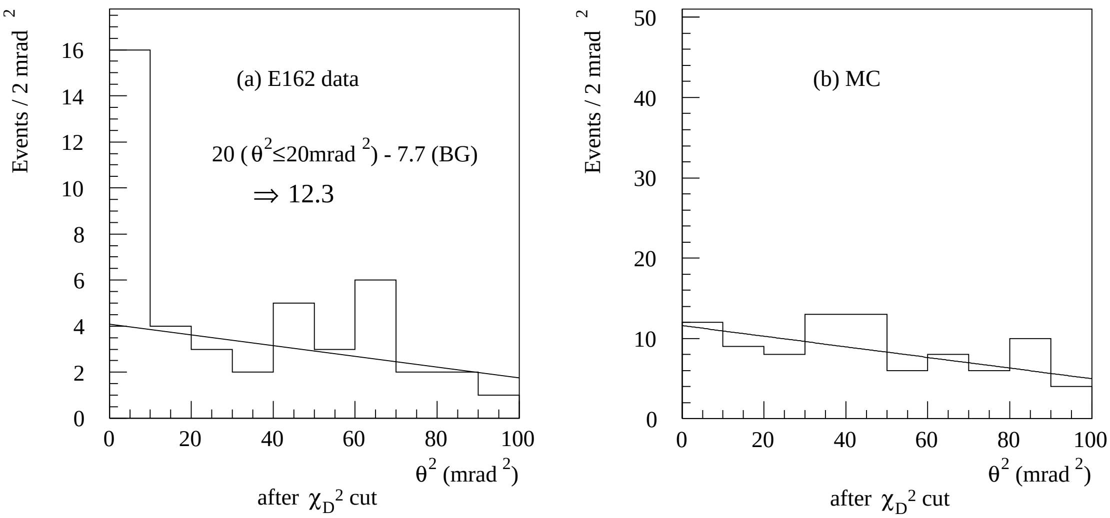

Fig. 8. Projection onto the θ^2 axis of the events with $M_{\pi\pi ee} > 450$ MeV/c^2.

4 Results

The branching ratio was calculated by

$$\begin{aligned}\mathrm{Br}(K_L \to \pi^+\pi^- e^+e^-) &= \mathrm{Br}(K_L \to \pi^+\pi^-\pi^0) \cdot \mathrm{Br}(\pi^0 \to e^+e^-\gamma) \\ &\times \frac{A(\pi^+\pi^-\pi^0_D)}{A(\pi^+\pi^-e^+e^-)} \cdot \frac{\eta(\pi^+\pi^-\pi^0_D)}{\eta(\pi^+\pi^-e^+e^-)} \cdot \frac{N(\pi^+\pi^-e^+e^-)}{N(\pi^+\pi^-\pi^0_D)},\end{aligned}$$

where A, η, and N denote acceptance, efficiency, and observed number of events, respectively. We employed Monte Carlo simulations to determine acceptances and detection efficiencies for the two processes. We note here that the acceptance and/or efficiencies for the $\pi^+\pi^-e^+e^-$ mode depend upon unknown amplitudes. In the following calculations, we assumed that there exist only two amplitudes, M1 and IB, with their relative strengths given in Ref. 1.

The acceptance obtained by the simulations was 0.64×10^{-3} for $\pi^+\pi^-\pi^0_D$ (Ref. 6) and 1.8×10^{-3} for $\pi^+\pi^-e^+e^-$. Differences in efficiency between $\pi^+\pi^-e^+e^-$ and $\pi^+\pi^-\pi^0_D$ originated from the detector response as well as kinematical cuts. As for the detector response, most of the efficiencies were common to the two modes. The exception was the efficiency related to the γ-ray in $\pi^+\pi^-\pi^0_D$. Its inefficiency, stemming mainly from clusters merging with other decay products, was found to be 20% as estimated by the Monte Carlo simulation. There existed several kinematical cuts which caused differences in efficiency for the two modes. The χ^2_D cut was applied only to the $\pi^+\pi^-e^+e^-$ mode, and its efficiency was found to be 95%. We rejected the events that contained $\pi^0 \to e^+e^-\gamma$ candidates for $\pi^+\pi^-e^+e^-$. The event loss due to over-veto was estimated by analyzing the properties of extra γ-rays in observed $\pi^+\pi^-\pi^0_D$ events and found to be 1%. The requirements for momenta (p_π) and asymmetry (A_{+-}) imposed on charged pions were also a source of the efficiency difference. We estimated that the combined efficiencies were 96% for $\pi^+\pi^-\pi^0_D$ and 88% for $\pi^+\pi^-e^+e^-$. All the other cuts were found to produce negligibly small effects. Finally, we used the known branching ratios for the normalization mode of $\mathrm{Br}(K_L \to \pi^+\pi^-\pi^0) = 0.1256$ and $\mathrm{Br}(\pi^0 \to e^+e^-\gamma) = 1.198 \times 10^{-2}$ (Ref. 7).

The result for the branching ratio is

$$\mathrm{Br}(K_L \to \pi^+\pi^-e^+e^-) = (5 \pm 2) \times 10^{-7} \quad (\mathit{Preliminary}).$$

Again the error is only statistical. The branching ratio obtained above is consistent with the theoretical prediction[1] and the result reported by the KTeV group.[5]

In conclusion, we searched for the decay mode $K_L \to \pi^+\pi^-e^+e^-$ with the 13 GeV/c proton synchrotron at KEK. We found 12 ± 5 events and obtained the branching ratio of $\mathrm{Br} = (5 \pm 2) \times 10^{-7}$. The result is still preliminary: we are now studying the systematic errors in detail and refining the analysis. We hope to publish the results soon.

Acknowledgments

First of all, I would like to thank all of my colleagues for making this experiment successful. Special thanks should go to Prof. H. Sugawara, Prof. S. Iwata, and Prof. K. Nakai for their support and encouragement. I thank the staff of the Mechanical Engineering Center at KEK, in particular Y. Higashi and Y. Funahashi, for their contributions in the construction of the detector. I also acknowledge the support from the operating crew of the Proton Synchrotron, members of the Beam Channel group, and the Computing Center at KEK.

References

[1] L. M. Sehgal and M. Wanninger, Phys. Rev. D **46**, 1035 (1992); **46**, 5209(E) (1992); P. Heilinger and L. M. Sehgal, *ibid.* **48**, 4146 (1993).

[2] D. P. Majumdar and J. Smith, Phys. Rev. **187**, 2039 (1969); J. K. Elwood, M. B. Wise, and M. J. Savage, Phys. Rev. D **52**, 5095 (1995); J. K. Elwood *et al.*, Phys. Rev. D **53**, 4078 (1996).

[3] M. Ya. Balats *et al.*, Sov. J. Nucl. Phys. **38**(4), 556 (1983).

[4] T. Nomura *et al.*, Phys. Lett. B **408**, 445 (1997).

[5] A preliminary result of $\mathrm{Br} = 2.6 \pm 0.5 \times 10^{-7}$ has been reported by the KTeV group based on 36.1 ± 6.4 events; a talk was presented by R. J. Tesarek at the JHF Workshop (1997).

[6] In the Monte Carlo simulation, we used the phase space for the $K_L \to \pi^+\pi^-\pi^0$ decay and the Kroll-Wada spectrum, N. M. Kroll and W. Wada, Phys. Rev. **98**, 1355 (1955), for the Dalitz decay.

[7] Particle Data Group, R. M. Barnett *et al.*, Phys. Rev. D **54**, 1 (1996).